



The influence of hatch spacing on the metallurgical characteristics of 17–4 PH stainless steel processed by DED

Ipfi Mathoho^{1,2} · Thabiso Sibisi³

Received: 28 August 2023 / Accepted: 23 November 2023 / Published online: 17 January 2024
© The Author(s) 2024

Abstract

The quality and performance of additively manufactured part is linked to the process parameters such as laser power, scanning speed, powder feed rate, and layer thickness. However, hatch spacing is one of the process parameters that affect the quality and performance of the part, but its effect has not been fully investigated. Therefore, this study seeks to investigate the effect of hatch spacing on the metallurgical characteristics, including microstructural evolution, microhardness, and corrosion behavior of 17–4 PH stainless produced through direct energy deposition. A LENS system was used to manufacture 17–4 PH SS cubes and the hatch overlap was varied from 20 to 80%. Subsequently, the printed cubes were subjected to heat treatment (H900) followed by material characterization which includes microstructural analysis, microhardness, and corrosion behavior. This study deduced that varying the percent overlap had an impact on the proportion of delta ferrite and the grain size. Furthermore, increasing the percent overlap from 20 to 80% was found to cause a reduction in hardness (340–331 HV). Meanwhile, it was found that traditionally manufactured 17–4 PH SS is more susceptible to corrosion than additively manufactured 17–4 PH SS.

Keywords 17–4 PH stainless steel · Corrosion · DED · Microhardness · Microstructure

1 Introduction

The American Society for Testing and Material (ASTM) [1] defines additive manufacturing (AM) as an advanced manufacturing technology that produces parts/objects based on a 3D computer-aided design (CAD) file by building layer upon layer [2–4]. Unlike its counterpart processes such as machining which manufactures parts by removing materials from the parent material [5, 6], AM over the years has been the driving vehicle of the fourth industrial revolution and is now making inroads in industries such as aerospace, biomedical,

automotive, and energy [7]. The penetration of AM to the aforementioned industries/markets is due to the fact that AM possesses attractive attributes which makes it a preferred candidate over its counterpart process. Such attributes include the ability to produce parts with complex geometry, parts with enhanced mechanical properties, and the ability to produce low-cost parts [8]. One of the commonly used AM technologies is called direct energy deposition (DED). This technique manufactures components by simultaneously irradiating the powder with a laser beam [8–10]. DED, as opposed to its counterpart processes such as selective laser melting, can produce functionally graded materials (FGMs) and can repair worn-out surfaces. However, DED like any other process has its fair share of weaknesses, i.e., DED produces parts with poor surface integrity and this can have detrimental effects on the parts when they are in service.

Researchers over the years have managed to study and report on the behavior of alloys such as titanium and iron based that were produced through the DED technique. However, there is a need to extend the depth of knowledge in relation to the relationship between process parameters (hatch spacing) and the metallurgical characteristics of 17–4 PH SS produced by DED. 17–4 PH stainless steel is a

✉ Ipfi Mathoho
imathoho@csir.co.za; imathoh@gmail.com

¹ Laser Enabled Manufacturing Group, National Laser Centre, Council for Scientific and Industrial Research, Pretoria Campus, Pretoria 0001, South Africa

² Department of Mechanical Engineering Science, Faculty of Engineering and the Built Environment, University of Johannesburg, Johannesburg 2006, South Africa

³ Department of Chemical, Metallurgical and Materials Engineering, Tshwane University of Technology, P.M.B. X680, Pretoria, South Africa

precipitation hardenable material with superior mechanical properties and outstanding corrosion resistance. 17–4 PH is widely used in engineering applications by industries such as aerospace, energy, and automotive because of the aforementioned characteristics [11, 12].

Dong et al. [13] conducted a study that focused on investigating the effect of hatch spacing on the microstructure of one layer. They found that increasing the hatch spacing resulted in an increase in the grain size and attributed this behavior to a reduced cooling rate. Meanwhile, Zhang et al. [14] investigated the effects of hatch spacing on the microstructure and anisotropy of 316 stainless steel cubes manufactured by laser powder bed fusion. Their findings were contrary to those of Dong et al. [13] in the sense that they argued that increasing the hatch spacing resulted in reduced grain size.

In addition, Schaller et al. [15] studied the corrosion behavior of 17–4 PH stainless steel manufactured by powder fusion. They found that 17–4 PH stainless steel manufactured through traditional methods is less prone to corrosion than 17–4 PH manufactured through powder bed system. They attributed this behavior to the presence of pores. Their findings corroborated those of Alnajjar et al. [16]; they also reported that wrought-produced 17-PH stainless steel outperformed re-austenitized selective melted 17–4 PH stainless steel, and their argument was that the latter had higher grain boundary density which promoted corrosion. Meanwhile, Bajaj et al. [16] reported that 3D-printed 17–4 PH SS showed better corrosion resistance than the wrought 17–4 PH SS, and both materials in solutionized and aged condition. This was argued to be due to the refined microstructure of 3D-printed 17–4 PH SS and also the presence of fine niobium carbides.

This study investigated the influence of hatch spacing on the metallurgical characteristics of additively manufactured 17–4 PH stainless steel, which includes microstructural evolution, microhardness, and corrosion behavior. The current study deduced that varying hatch spacing does have

an influence on the proportion of delta ferrite, while it was also found that reducing hatch spacing (increasing % overlap) reduced microhardness. With regard to corrosion, it was found that the traditionally manufactured 17–4 PH SS in H900 condition is less resistant to corrosion than 3D-printed 17–4 PH SS in H900 condition.

2 Materials and methods

Figure 1 shows an SEM image of 17–4 PH stainless steel powder used to build the samples on the DED system. The elemental composition of 17–4 PH stainless steel powder obtained using EDS is shown in Table 1.

The powder shown in Fig. 1 was supplied by Weartech and had a particle size range of 45–90 μm . This powder was used to manufacture four samples with a dimension of $10 \times 10 \times 10$ mm on the 850-R Optomec LENS Platform. The four samples were manufactured using the set of parameters shown in Table 2, and processing was done while varying the hatch overlap from 20 to 80% and keeping constant the laser power, scanning speed, and powder feed rate. Subsequent to the manufacturing of the samples, they were subjected to material characterization which includes microstructural analysis, microhardness, and corrosion test. Kallings reagent was used to etch the samples to reveal the microstructure. Subsequently, the samples were analyzed by optical microscope (Olympus BX51 M) and scanning electron microscope (JEOL, JSM-6010Plus/LAM). Moreover, X-ray diffraction (XRD) was conducted to detect the phases present in the samples. This was done while using the scanning step size of 0.04° within a 2θ range of 10 to 100° . The systems employed a Cu source which was excited at the current 40 mA and voltage 54 kV. The samples were also subjected to a hardness test, and this test was done using Zwick/Roell ZHVm Vickers' microhardness tester.

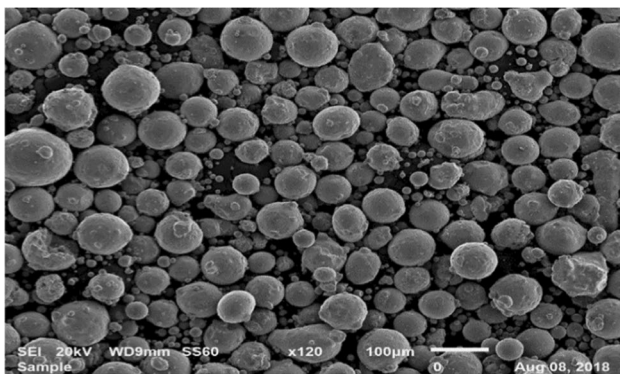


Fig. 1 17–4 PH stainless steel powder particles

Table 1 Elemental composition of 17–4 PH stainless steel powder

Elements	Fe	Cr	Ni	Cu	Si
Mass (%)	74.35	17.55	3.83	3.61	0.65

Table 2 LENS process parameters

Laser power (W)	Scanning speed (mm/s)	Powder feed rate (g/min)	Hatch overlap (%)
300	10.16	4.7	20
300	10.16	4.7	40
300	10.16	4.7	60
300	10.16	4.7	80

The samples experienced a load of 300gf for 10 s along the build direction planes. In addition, an H900 heat treatment was performed. This heat treatment involved two steps; the first step was to heat treat the samples to 1040 °C for 30 min followed by air cooling, while during the second step (aging) the samples were heat treated at 480 °C for 1 h followed by air cooling. Therefore, all the material characterizations highlighted above were also done for the samples in heat-treated condition. Lastly, a corrosion test was conducted on the as-built samples. Potentiostat DY2300, supplied by Digi-ivy, was used to do a corrosion test. The samples were immersed in 150 ml of sodium chloride (NaCl) for 2 h at room temperature.

3 Results and discussion

3.1 Microstructural evolution

Figure 2 shows the microstructures of 17–4 PH stainless steel in an as-built condition at various percent overlaps (20–80%). It was observed that the microstructure consisted of a mixture of delta ferrite and martensite when the hatch overlap was set at 20–60%. However, the microstructure that was observed at 80% overlap consisted of martensite only. The absence of delta ferrite at 80% overlap is due to the fact

that 80% of the previously built track was overlapped. Therefore, this suggests that the overlapped track will experience in situ heat treatment which will consequently lead to the delta ferrite dissolving. The effect of in situ heat treatment at 80% can also be supported by the fact that the microstructure at 80% overlap seems to be homogenous as opposed to the microstructure at 20, 40, and 60% overlaps.

To identify delta ferrite, localized EDS was used to measure its composition and that of the matrix and the EDS composition as expected shows that the amount of chromium is higher in delta ferrite than in the matrix as shown in Fig. 3. This ratio is expected because delta ferrite is rich in chrome. In addition, with the aid of SEM, it was observed that when the percent overlap was increased from 20 to 80%, the grain size increased. This behavior can be attributed to the fact that increasing percent overlap results in heat retention during printing, as it is generally known that heat retention favors grain growth, hence the observed grain growth in Fig. 4.

Moreover, the XRD patterns in Fig. 5 corroborate with the observations of microstructure in Fig. 2. This is because the XRD patterns show that at all percent overlaps, martensite is the only phase present. However, the delta ferrite observed in the microstructure is not visible on the XRD patterns because delta ferrite is body centered cubic (BCC) phase while martensite is a body centered tetragonal (BCT). Therefore, it is difficult for the XRD

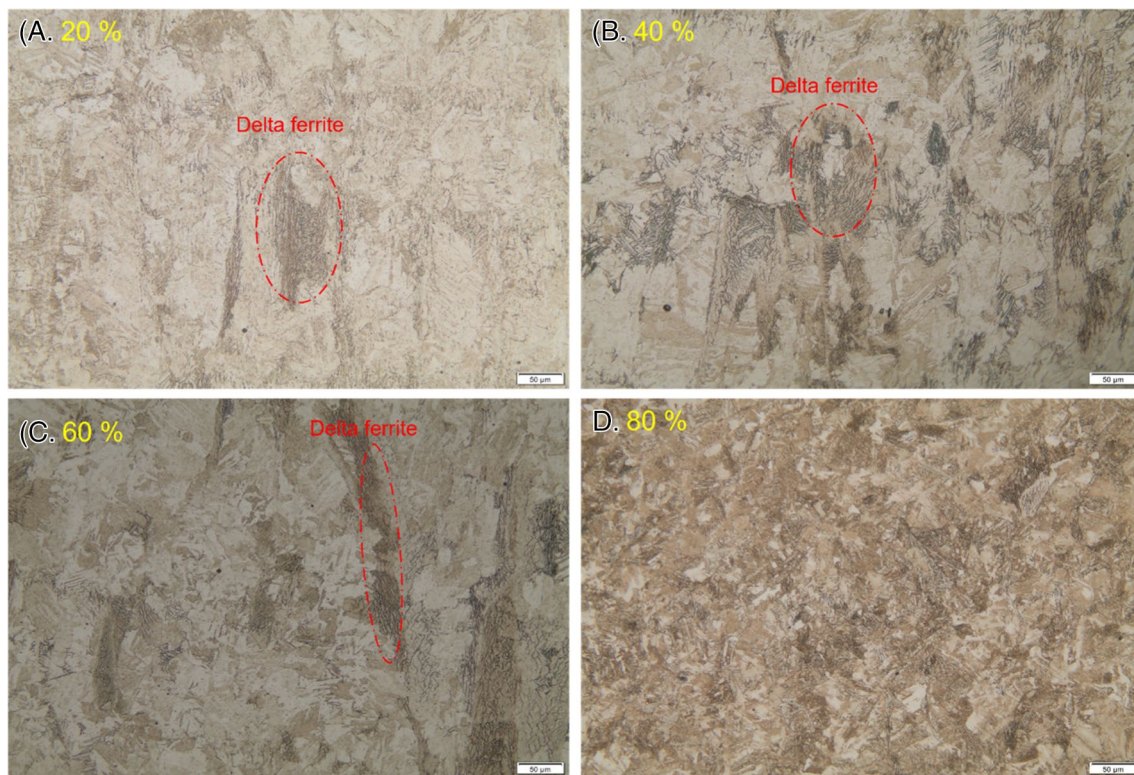


Fig. 2 OM as-built images of various % overlaps

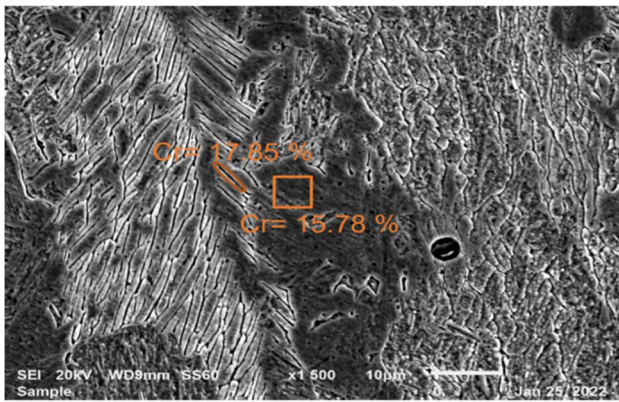


Fig. 3 Localized EDS results showing chrome composition in δ -ferrite and the matrix

analysis to differentiate the two phases, hence only martensite is shown on the XRD patterns. On the other hand, other studies such as the one conducted by Mathoho et al. [18] found that the microstructure in an as-built condition had a mixture of martensite and retained austenite according to their XRD patterns. This suggests that the cooling of the samples in the current study was rapid enough to avoid the retention of austenite.

3.2 Microhardness

The graph in Fig. 6 shows the microhardness profile and build height as a function of percent hatch overlap. The current study found that the hardness decreased when the percent overlap was increased from 20 to 80%. This behavior is supported by the microstructures shown in Fig. 2. This is because delta ferrite seems to dissolve back into the solution as the percent overlap is increased, and it is known that the presence of delta ferrite enhances the hardness. Therefore, it can be deduced that the reduction of hardness as a result of increasing percent overlap can be attributed to the delta ferrite dissolving back into solution. Another possible contributing factor to the reduction of hardness as a result of increasing percent overlap may be caused by the in situ tempering of martensite. As shown by the graph in Fig. 6, the increase of build height after printing is also an indication of the possibility of in situ tempering of martensite.

3.3 Heat treatment

After printing, the samples were subjected to condition A heat treatment followed by aging treatment (H900 condition). The microstructure, microhardness, and corrosion in as-built, condition A, and H900 were contrasted.

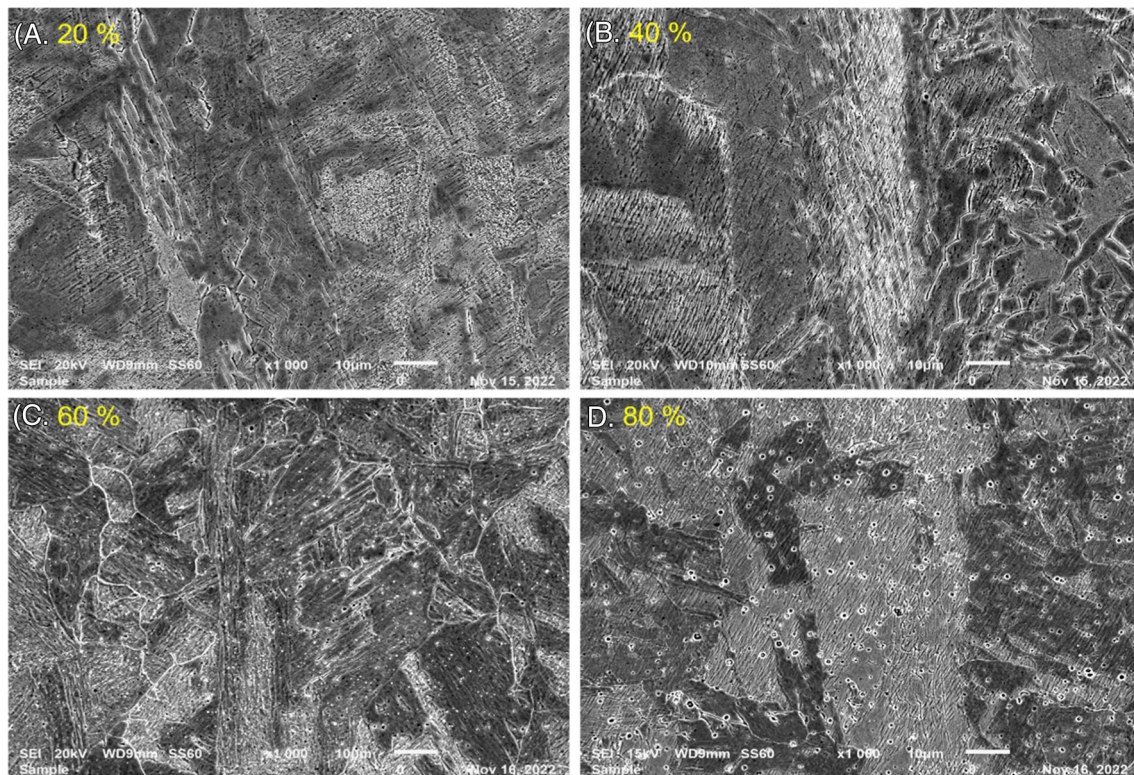


Fig. 4 SEM as-built images of various % overlaps

M: Martensite

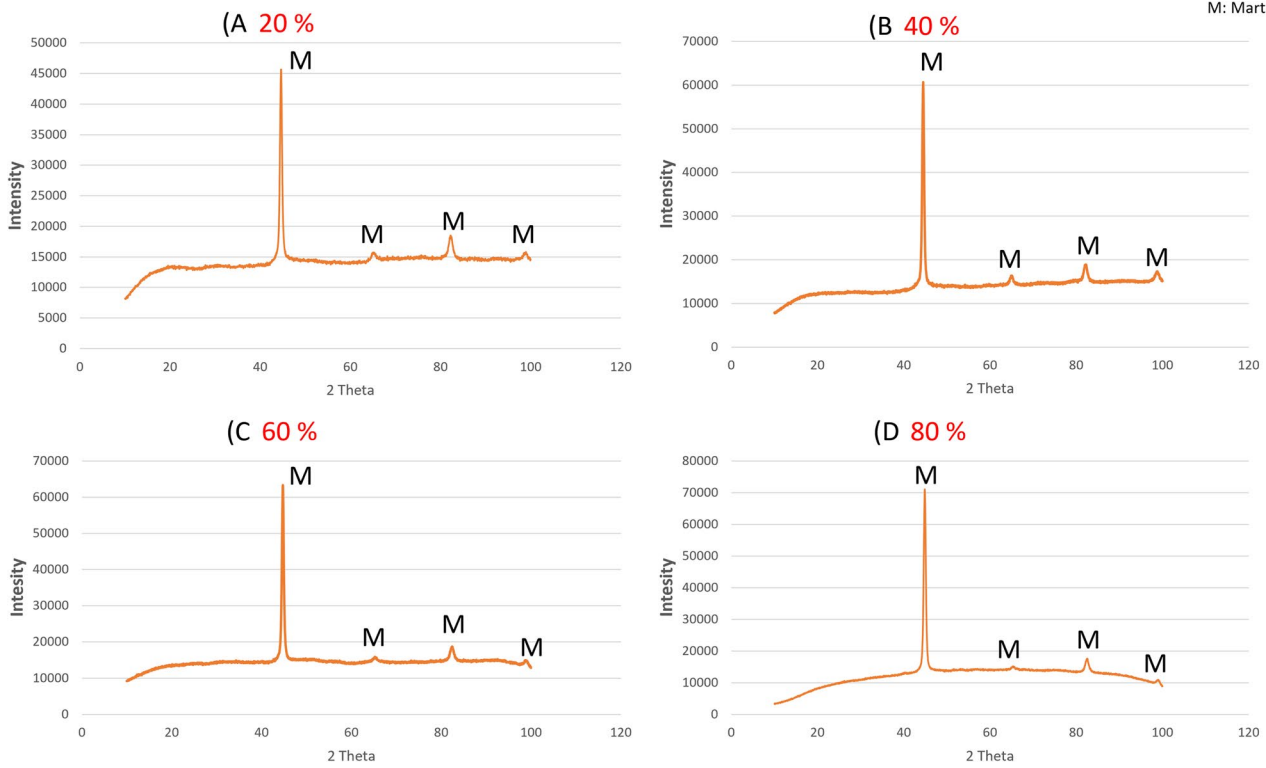
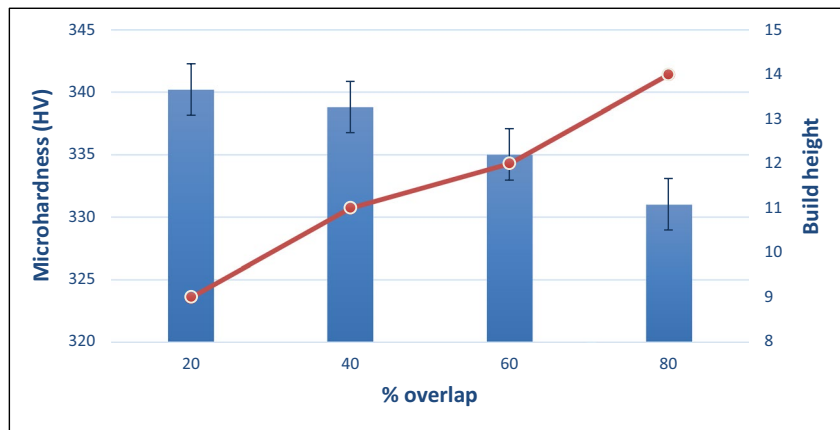


Fig. 5 XRD patterns at various % overlaps

Fig. 6 Microhardness at various % overlaps



3.3.1 Microstructural evolution

Figure 7 shows the microstructures in various conditions, i.e., as-built, condition A, and H900. As reported above, the microstructure in as-built condition consisted of delta ferrite and martensite. However, Fig. 7 shows that after applying condition A, delta ferrite was dissolved and the microstructure became homogenized. When the samples were subjected to the H900 condition, the microstructure became coarser; it is worth highlighting that the aforementioned behavior that was observed in all percent overlaps varied.

This behavior is clearly shown by SEM microstructures in Fig. 8. According to the XRD patterns shown in Fig. 9, it can be seen in all the samples that after being subjected to H900 condition, the microstructure consisted of martensite only.

3.3.2 Microhardness

Figure 10 shows the graph of microhardness at various percent overlaps and in various conditions. It was found that when all the samples were subjected to condition A, the microhardness decreased slightly, and this behavior can be

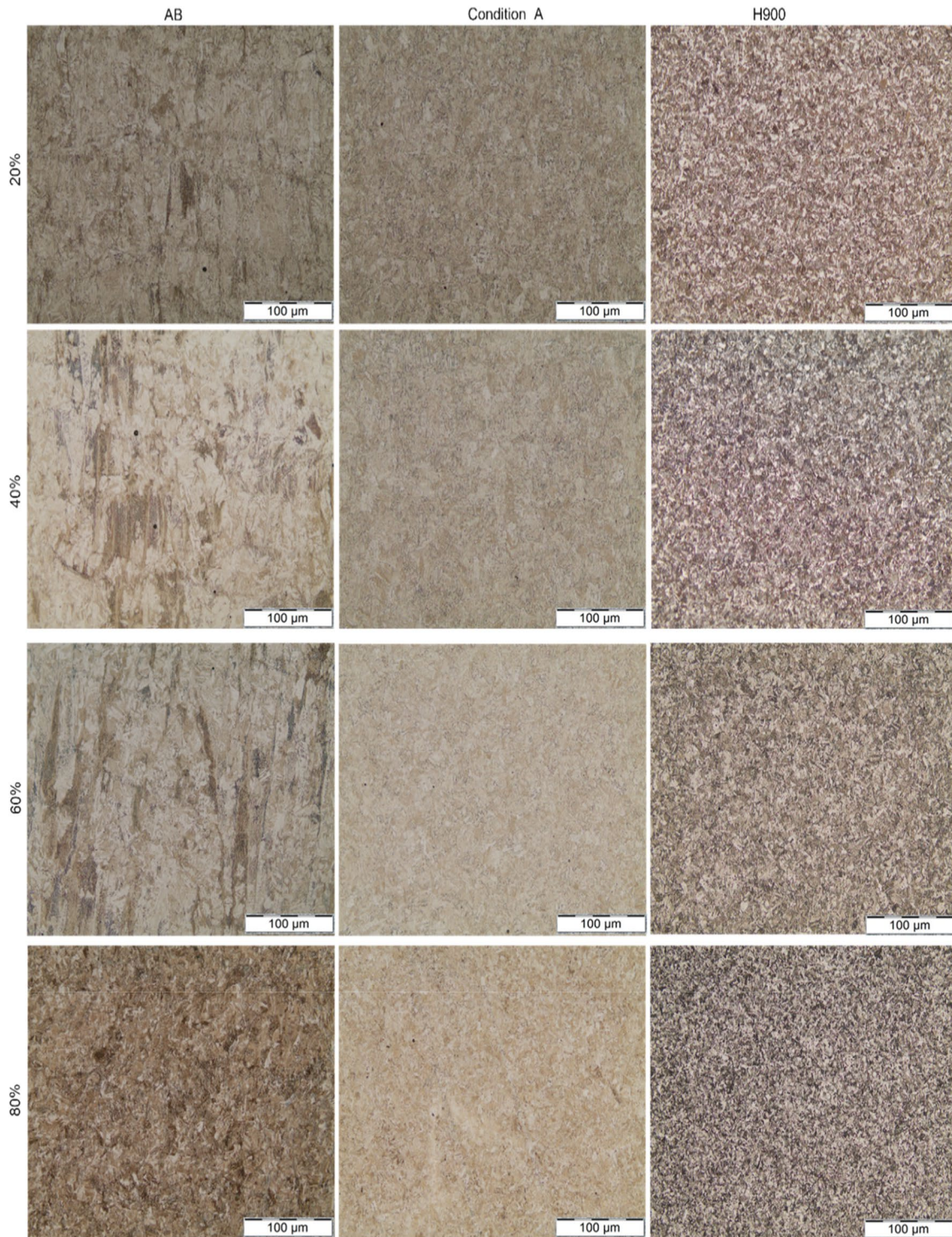


Fig. 7 OM microstructures in various conditions (AB, condition A, and H900)

attributed to the fact that delta ferrite which was present in the as-built condition was dissolved after condition A, and it is known that the presence of delta ferrite causes an increase in hardness. Furthermore, Fig. 10 shows that after subjecting the samples to the H900 condition, the hardness increased

and this is attributed to the precipitation of nano-scale CU precipitates. These precipitates increase the hardness by hindering dislocation movement. These precipitates could not be observed using SEM and require high-resolution equipment such as the transmission emission microscope (TEM).

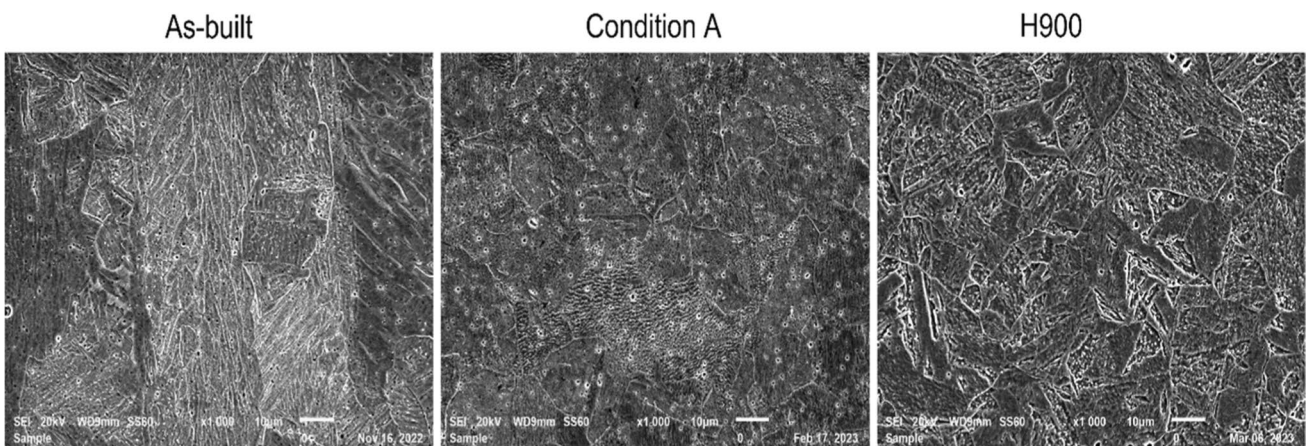


Fig. 8 The microstructure at various conditions (as-built, condition A, and H900) of 60% overlap

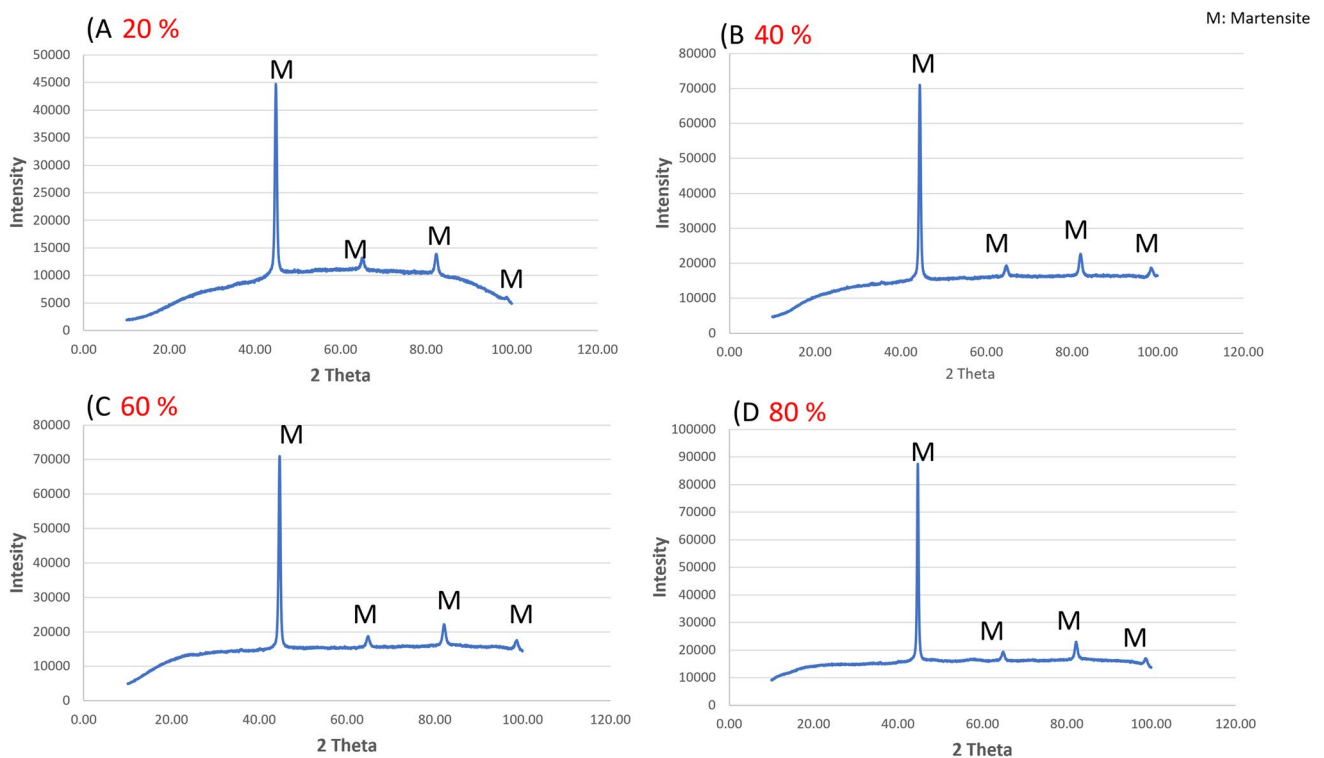


Fig. 9 XRD patterns after heat treatment at various overlaps

3.4 Corrosion behavior

Table 3 shows corrosion results conducted on as-built (AB), 40% overlap subjected to H900 condition (HT), and casted 17–4 PH subjected to H900 condition (AR). The results show that AB has the least current density and low corrosion, and this implies that AB is the most corrosion-resistant sample. However, after subjecting it to H900, it was found that the corrosion resistance was compromised or reduced. This might be due to the fact that aging causes

the precipitation of copper from the matrix and since copper reduces the susceptibility to corrosion as a result, the matrix will be less corrosion resistant. Moreover, Table 3 shows that casted 17–4 PH in H900 condition is more prone to corrosion than 3D-printed 17–4 PH in H900 condition; this behavior is corroborated by findings obtained from a study conducted by Alnajjar et al. [16].

Figure 11 shows that both the AR and the AB started by corroding from the start of the test and then stabilized just after 1000 s. However, the HT curve started by passivating,

Fig. 10 Microhardness of different conditions at 20, 40, 60, and 80% overlaps

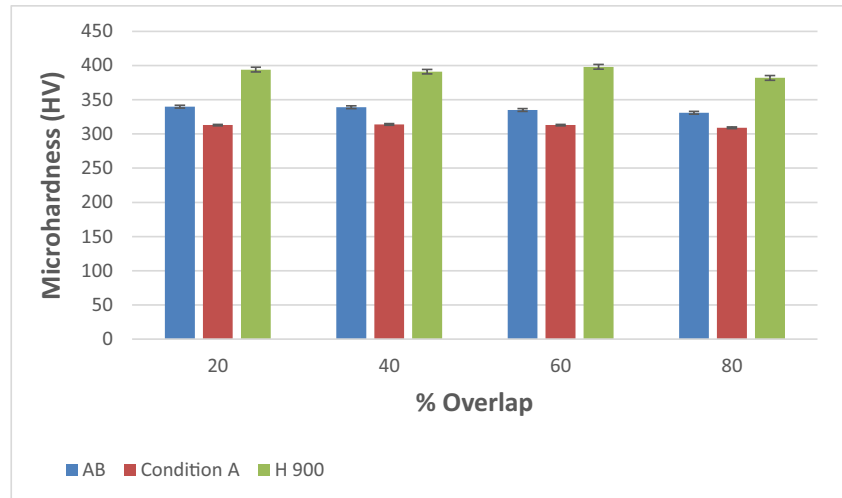


Table 3 Corrosion results

Sample	j_{corr} (A/cm ²)	E_{corr} (V)	Corrosion rate (mm/year)
AB	1.9299E-08	-0.35186	0.00022425
HT	5.9595E-05	-0.34008	0.69249
AR	8.2617E-05	-0.2665	0.96

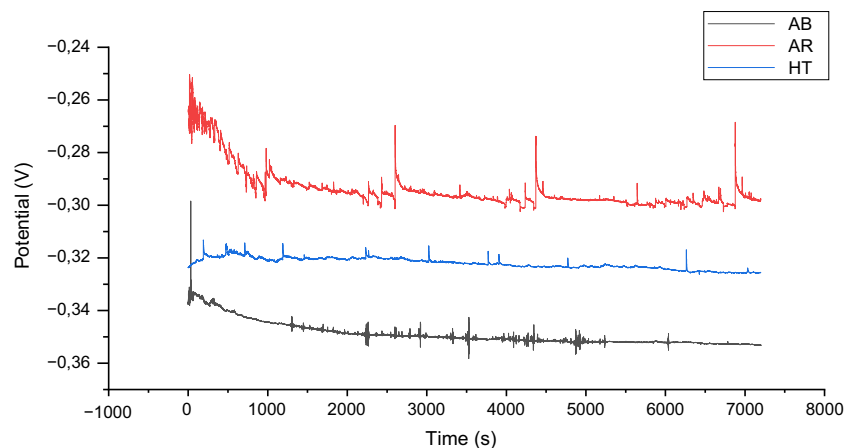
and after a short while just before 500 s, it stabilized. Akainlabi et al. [17] reported that the more the material possesses more positive potential, the more corrosion resistant that particular material will be. Figure 11 shows that both the AR and the AB started by corroding from the start of the test and then stabilized just after 1000 s. However, the HT curve started by passivating, and after a short while just before 500 s, it stabilized.

The Tafel curves in Fig. 12 show that there is not a large variation among the three samples in relation to the potential. However, AR seems to have the least corrosion

resistance while AB seems to be the most corrosion resistant among the three samples. This is corroborated by the current density which shows that AR recorded the highest current density while AB recorded the least current density. Swietlickinet et al. [19] argued that small grains promote more corrosion nucleation sites, which eventually lead to corrosion. However, the current study does not agree with that argument because Fig. 13 shows that AB had the smallest grain size (19 μm) while AR had the largest grain size (73 μm).

Figure 14 shows SEM of corroded surface for samples in as-built, H900, and as-received conditions. It can be seen that all the samples are experiencing the same type of corrosion, which is pitting corrosion. Furthermore, it was discovered that in AB and HT samples the pitting corrosion observed was localized and it occurred in areas adjacent to delta ferrite. Since delta ferrite is known to be supersaturated with chrome, and chrome is known to enhance corrosion resistance, this implies that areas adjacent to delta ferrite will be less in chrome which will consequently result in those areas being prone to corrosion. With the aid

Fig. 11 OCP curves of different samples



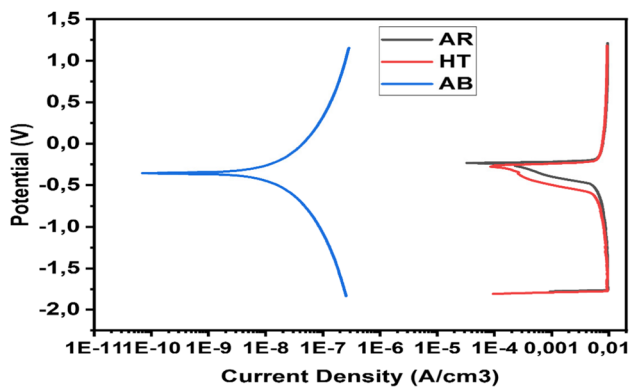


Fig. 12 Tafel curves of different samples (AB, HT, and AR)

of localized EDS, this argument was corroborated as seen in Fig. 14 with the amount of chrome in corroded areas and the matrix.

4 Conclusion

The current study deduced that varying percent overlap had an impact on the proportion of delta ferrite. In addition, increasing percent overlap resulted in an increment of grain size; this was due to heat retention caused by high percent overlap. On the other hand, it was established that increasing percent overlap reduced the hardness. This behavior was linked to the reduction of delta ferrite as percent overlap was increased because the martensite in the section that has already solidified will experience tempering due to heat retention.

Furthermore, it was established that solution treatment resulted in dissolving delta ferrite back into the solution. With regards to the effect of heat treatment, it was found that the solution treatment reduced hardness while the aging treatment increased the hardness in all the samples.

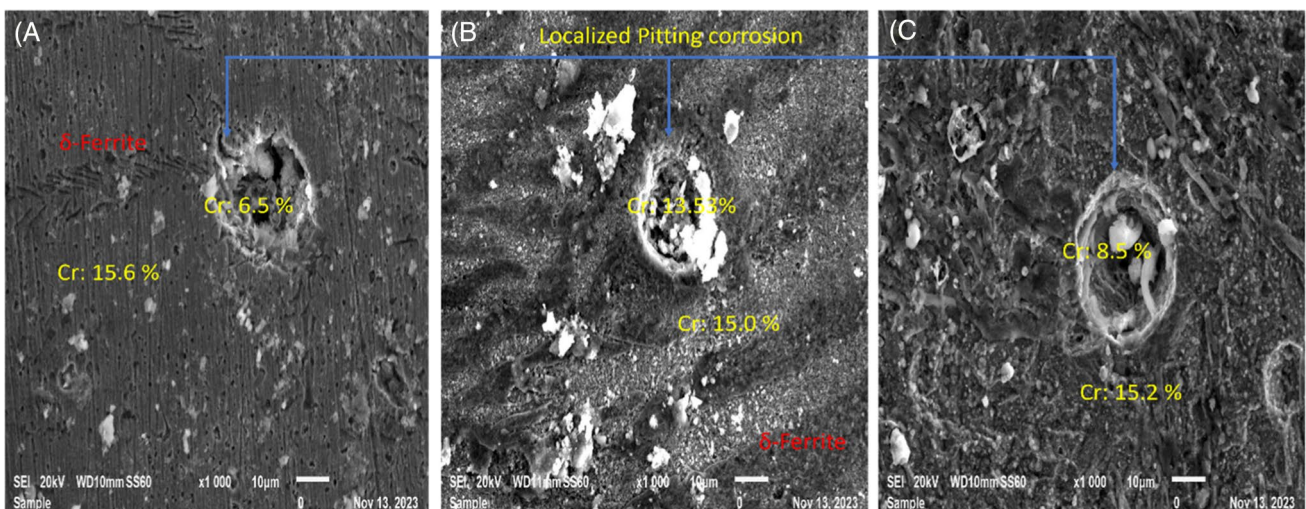
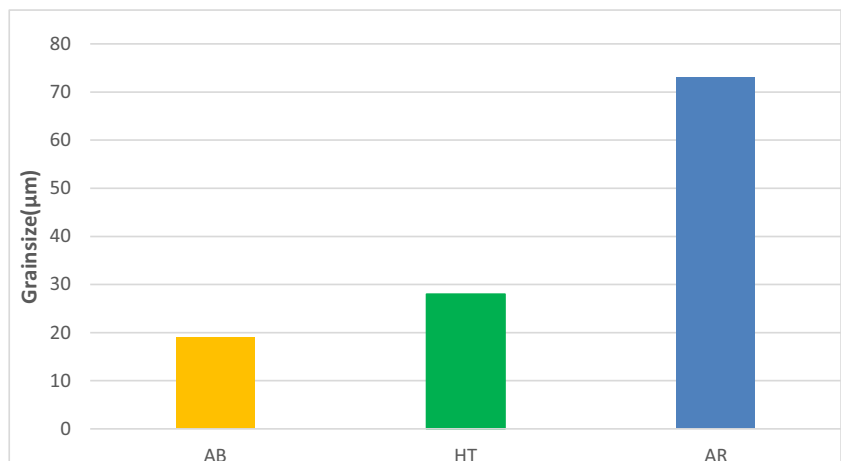


Fig. 13 Corroded surface of SEM images: (A, B) AB, (C) HT

Fig. 14 Grain size of different samples (AB, AR, and HT)



As for corrosion, the current study deduced that 3D-printed 17-4 PH in an as-built condition is less susceptible to corrosion than heat-treated 17-4 PH produced through 3D printing. Interestingly, it was deduced that casted 17-4 PH in H900 condition is more prone to corrosion than 3D-printed 17-4 PH in H900 condition.

Acknowledgements The authors thank the National Research Foundation for their financial support and Tshwane University of Technology for the use of their potentiostat.

Author contribution All authors contributed to the study conception and design. Material preparation, data collection, and analysis were performed by IM and TS. The first draft of the manuscript was written by IM and all authors commented on previous versions of the manuscript. All authors read and approved the final manuscript.

Funding Open access funding provided by Council for Scientific and Industrial Research. This work was supported by the National Research Foundation (grant no. 138316 awarded to IM).

Declarations

Conflict of interest The authors declare no competing interests.

Open Access This article is licensed under a Creative Commons Attribution 4.0 International License, which permits use, sharing, adaptation, distribution and reproduction in any medium or format, as long as you give appropriate credit to the original author(s) and the source, provide a link to the Creative Commons licence, and indicate if changes were made. The images or other third party material in this article are included in the article's Creative Commons licence, unless indicated otherwise in a credit line to the material. If material is not included in the article's Creative Commons licence and your intended use is not permitted by statutory regulation or exceeds the permitted use, you will need to obtain permission directly from the copyright holder. To view a copy of this licence, visit <http://creativecommons.org/licenses/by/4.0/>.

References

- Standard ASTM (2012) Standard terminology for additive manufacturing technologies. ASTM International F2792–12a, pp 1–9
- Kumar S, Pityana S (2011) Laser-based additive manufacturing of metals. *Adv Mater Res* 227:92–95 (Trans Tech Publications Ltd)
- Mathoho I, Akinlabi ET, Arthur N, Tlotleng M, Masina B (2019) Metallurgical characteristics of laser peened 17-4 PH SS processed by LENS technique. In: TMS 2019 148th Annual Meeting & Exhibition Supplemental Proceedings, Springer International Publishing, pp 279–285
- Pinkerton AJ (2016) Lasers in additive manufacturing. *Opt Laser Technol* 1(78):25–32
- Akinlabi ET, Mathoho I, Mubiayi MP (2019) Corrosion behaviour and microhardness during dry and flood milling of Ti-6Al-4V alloy. *Key Eng Mater* 796:91–96
- Akinlabi ET, Mathoho I, Mubiayi MP, Mbohwa C, Makhatha ME (2018) Effect of process parameters on surface roughness during dry and flood milling of Ti-6Al-4V. In: 2018 IEEE 9th International Conference on Mechanical and Intelligent Manufacturing Technologies (ICMIMT), IEEE, pp 144–147
- Herderick E (2011) Additive manufacturing of metals: a review. *Mater Sci Technol* 16:1413
- Thompson SM, Bian L, Shamsaei N, Yadollahi A (2015) An overview of direct laser deposition for additive manufacturing; part I: transport phenomena, modeling, and diagnostics. *Addit Manuf* 8:36–62
- Saboori A, Gallo D, Biamino S, Fino P, Lombardi M (2017) An overview of additive manufacturing of titanium components by directed energy deposition: microstructure and mechanical properties. *Appl Sci* 9:883
- Zhu YY, Tang HB, Li Z, Xu C, He B (2019) Solidification behavior and grain morphology of laser additive manufacturing titanium alloys. *J Alloy Compd* 10:712–7166
- Hu Z, Zhu H, Zhang H, Zeng X (2017) Experimental investigation on selective laser melting of 17–4PH stainless steel. *Opt Laser Technol* 87:17–25
- Rafi HK, Pal D, Patil N, Starr TL, Stucker BE (2014) Microstructure and mechanical behavior of 17–4 precipitation hardenable steel processed by selective laser melting. *J Mater Eng Perform* 12:4421–4428
- Dong Z, Liu Y, Wen W, Ge J, Liang J (2018) Effect of hatch spacing on melt pool and as-built quality during selective laser melting of stainless steel: modeling and experimental approaches. *Materials* 12(1):50
- Zhang Z, Wang S, Liu H, Wang L, Xiao X (2023) Effects of hatch distance on the microstructure and mechanical anisotropy of 316 L stainless steel fabricated by laser powder bed fusion. *J Mater Eng Perform* 32(10):4757–4767
- Schaller RF, Taylor JM, Rodelas J, Schindelholz EJ (2017) Corrosion properties of powder bed fusion additively manufactured 17–4 PH stainless steel. *Corrosion* 73(7):796–807
- Alnajjar M, Christien F, Barnier V, Bosch C, Wolski K, Fortes AD, Telling M (2020) Influence of microstructure and manganese sulfides on corrosion resistance of selective laser melted 17–4 PH stainless steel in acidic chloride medium. *Corros Sci* 168:108585
- Bajaj P, Hariharan A, Kini A, Kürnsteiner P, Raabe D, Jäggle EA (2020) Steels in additive manufacturing: a review of their microstructure and properties. *Mater Sci Eng: A* 772:138633
- Mathoho I, Akinlabi ET, Arthur N, Tlotleng M (2020) Impact of DED process parameters on the metallurgical characteristics of 17–4 PH SS deposited using DED. *CIRP J Manuf Sci Technol* 31:450–458
- Świetlicki A, Walczak M, Szala M (2023) Effect of shot peening on corrosion resistance of additive manufactured 17–4PH steel. *Mater Sci-Pol* 40(3):135–151

Publisher's Note Springer Nature remains neutral with regard to jurisdictional claims in published maps and institutional affiliations.